Noiseless linear amplification in quantum target detection using Gaussian states

Athena Karsa, Masoud Ghalaii, and Stefano Pirandola
Department of Computer Science, University of York, York YO10 5GH, UK
(Dated: January 10, 2022)

Quantum target detection aims to utilise quantum technologies to achieve performances in target detection not possible through purely classical means. Quantum illumination is an example of this, based on signal-idler entanglement, promising a potential 6 dB advantage in error exponent over its optimal classical counterpart. So far, receiver designs achieving this optimal reception remain elusive with many proposals based on Gaussian processes appearing unable to utilise quantum information contained within Gaussian state sources. This paper considers the employment of a noiseless linear amplifier at the detection stage of a quantum illumination-based quantum target detection protocol. Such a non-Gaussian amplifier offers a means of probabilistically amplifying an incoming signal without the addition of noise. Considering symmetric hypothesis testing, the quantum Chernoff bound is derived and limits on detection error probability is analysed for both the two-mode squeezed vacuum state and the coherent state classical benchmark. Our findings show that in such a scheme the potential quantum advantage is amplified even in regimes where quantum illumination alone offers no advantage, thereby extending its potential use. For coherent states, the performance in such a scheme is bounded by one without amplification except for a few specific regimes which are defined.

I. INTRODUCTION

Quantum mechanics, and the non-classical phenomena arising from it, have revolutionised many modern technologies including computation [1–3], communication [4–6] and sensing [7]. Quantum target detection forms a particular subset of quantum sensing protocols in which ones aim is to determine whether or not a target is present in some region of interest. Quantifying one's capability of doing so, and also confirming the benefits of using a quantum strategy, is carried out on the analysis of bounds on the probability of an error, in particular, comparing the upper bound to the lower bound of the corresponding, optimal classical method. Typically this classical benchmark will take the form of a coherent state, a quantum state with minimum uncertainty, with homodyne detection at the receiver.

Quantum illumination (QI) [8–10] is one of the first proposed protocols for quantum target detection. The protocol begins by generating an entangled source comprising two modes where one is designated the role of 'signal', and sent to probe the target region, while the other takes the role of the 'idler' and is retained for later joint-measurement at the receiver. Remarkably, QI offers a quantum advantage in target detection despite the fact that decoherence of entanglement is encoded into the protocol itself. This quantum advantage is maximal under constraints of low signal-brightness, low target reflectivity and high background noise. Within such a regime the effective signal-to-noise ratio (SNR) of such an entangled-source transmitter offers a factor of 4 advantage over that of the corresponding classical benchmark of coherent states with homodyne detection, equivalent to a 6 dB improvement in error exponent.

Attainment of this well-known 6 dB quantum advantage through QI relies on the use of an optimal joint-measurement, however, the details of such a measurement remains unknown. Various receiver designs have been proposed for QI: the phase-conjugating (PC) and optical parametric amplification (OPA) [11] achieve, at most, a 3 dB performance enhancement over coherent states while a receiver based on sum-frequency generation with feed forward (FF-SFG) [12] is capable of saturating the quantum Chernoff bound (QCB) for QI, though this receiver remains technologically out of reach. Experimentally, receivers are generally based on homodyne-type measurements carried out on the modes to determine the state's quadrature values. Owing to the uncertainty principle, such measurements necessarily introduce noise to the system. Further, since homodyne statistics are described by marginals of the Wigner function of a state which is a classical probability distribution. As such, any homodyne-type measurement on a Gaussian state, whose Wigner function is positive, results in a description of quadratures which is realistic, i.e., not purely quantum-mechanical, and thus unable to demonstrate any violation of Bell inequalities. Nonetheless, Gaussianity offers straightforward means of experimental implementation, with tools associated with Gaussian state generation, transformation and detection readily available in optics labs. As such, one could consider as an alternative either using non-Gaussian measurements on Gaussian states or Gaussian measurements on non-Gaussian states.

One of the proposed solutions to fight loss in communication links is to use amplifiers. While standard, Gaussian amplifiers can effectively recover losses in a classical signal, they necessarily add noise to the system rendering the resultant effective SNR bounded by the original such that no overall gains in performance can be achieved. Noiseless linear amplifiers (NLAs) offer a non-Gaussian means of non-deterministically amplifying a quantum state without the addition of noise, at the expense that when the procedure fails the signal is projected onto the vacuum state and completely lost [13–16]

(interested readers are referred to Ref. [17] for a review). Experimentally, different NLA modules have been realized successfully [18–20]. Previously, NLAs have been shown to demonstrate an increased robustness against loss and noise in continuous-variable quantum key distribution [21–24] and quantum repeater [25–27] protocols allowing for an increase in maximum transmission distance. They have also been shown to improve the performance of quantum distillation protocols [28, 29] and quantum enhancement of signal-to-noise ratio [30].

In this paper we consider the use of an NLA at the detection stage of the QI protocol, effectively creating a non-Gaussian receiver, which naturally post-selects signals, for QI with a Gaussian probe. Then, by mapping the protocol of QI with a two-mode squeezed vacuum (TMSV) state with an NLA to one without an NLA but transformed Gaussian state input and quantum channel parameters, we compute the QCB. Considering the same procedure for the classical benchmark of coherent states, we show that under appropriate parameter constraints, an enhanced quantum advantage may be achieved. In particular, the resultant performance of a post-quantum channel NLA on a coherent state is almost always upper-bounded by the performance of a coherent state without the NLA. There exists certain regimes, specified in terms of background level and target reflectivity, within which there are particular values of NLA gain for which an advantage over non-NLA coherent state protocols can be found. On the other hand, the NLA acting on the received TMSV quantum channel output always yields an enhancement in detection capabilities.

II. NOISELESS LINEAR AMPLIFICATION FOR QI

A. The QI protocol

Consider the production of M independent signal-idler mode pairs, $\{\hat{a}_S^{(k)}, \hat{a}_I^{(k)}\}$; $1 \leq k \leq M$, with mean number of photons per mode N_S for each of the signal and idler modes, respectively. The signal (S) mode is sent out to some target region while the idler (I) mode is retained at the source for later joint measurement. Their joint state, $\hat{\rho}_{S,I}$, is modelled as a two-mode, zero-mean Gaussian state [31] with covariance matrix (CM) given by

$$\mathbf{V}_{S,I} = \begin{pmatrix} \nu\mathbf{1} & c_q\mathbf{Z} \\ c_q\mathbf{Z} & \nu\mathbf{1} \end{pmatrix}, \quad \begin{cases} \mathbf{1} := \mathrm{diag}(1,1), \\ \mathbf{Z} := \mathrm{diag}(1,-1), \end{cases} \tag{1}$$

where $\nu := 2N_S + 1$ and $c_q = 2\sqrt{N_S(N_S+1)}$ quantifies the quadrature correlations between the two modes. The off-diagonal terms can in fact take any value such that $0 \leq c \leq 2\sqrt{N_S(N_S+1)}$. In the case where the signal-idler mode pairs are maximally entangled we have $c = c_q := 2\sqrt{N_S(N_S+1)}$ (the TMSV state [31]) while the case $c = c_d := 2N_S$ renders the state just-separable [32, 33].

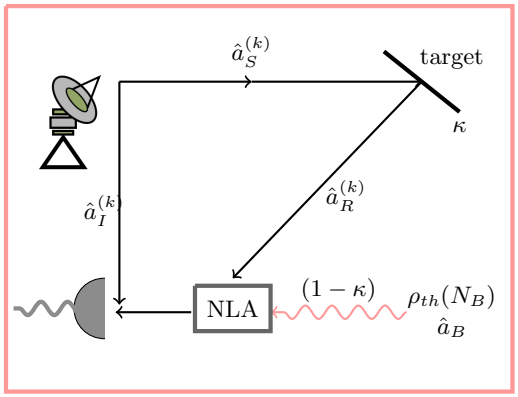

FIG. 1: Protocol for QI with the use of NLA at the detector. M independent signal-idler source mode pairs are generated with annihilation operators $\hat{a}_S^{(k)}$ and $\hat{a}_I^{(k)}$, respectively, with $1 \leq k \leq M$. The signal mode is sent to probe the target region in which target of reflectivity κ is equally-likely to be present or absent while the idler mode is sent straight to the receiver. At the receiver, the returning signal, mixed with the ambient background $\hat{a}_B$, first encounters an NLA which probabilistically noiselessly amplifies it before recombination with the idler in the decision-making process.

Under hypothesis H_0, the target is absent so that the returning mode $\hat{a}_R = \hat{a}_B$, where $\hat{a}_B$ is in a thermal state with mean number of photons per mode N_B. Under hypothesis H_1, the target is present such that $\hat{a}_R = \sqrt{\kappa}\hat{a}_S + \sqrt{1-\kappa}\hat{a}_B$. Here, κ is the target reflectivity, incorporating all propagation losses associated with the channel, and $\hat{a}_B$ is in a thermal state with mean number of photons per mode $N_B/(1-\kappa)$, so that the mean noise photon number is equal under both hypotheses (no passive signature). The conditional joint state, $\hat{\rho}_{R,I}^i$ for $i = 0, 1$, of the returning (R) mode and the retained idler (I) is given by, under hypotheses H_0 and H_1, respectively,

$$\mathbf{V}_{R,I}^0 = \begin{pmatrix} \omega\mathbf{1} & 0 \\ 0 & \nu\mathbf{1} \end{pmatrix}, \tag{2}$$

$$\mathbf{V}_{R,I}^1 = \begin{pmatrix} \gamma\mathbf{1} & \sqrt{\kappa}c_q\mathbf{Z} \\ \sqrt{\kappa}c_q\mathbf{Z} & \nu\mathbf{1} \end{pmatrix}, \tag{3}$$

where we set $\omega := 2N_B + 1$ and $\gamma := 2\kappa N_S + \omega$.

B. NLA action and effective parameters for QI

Consider the entanglement-based QI protocol where the source is a TMSV state comprising signal and idler modes given by

$$|\lambda\rangle_{S,I} = \sqrt{1-\lambda^2}\sum_{n=0}^{\infty}\lambda^n |n\rangle_S |n\rangle_I, \tag{4}$$

with $\lambda^2 = \frac{N_S}{N_S+1} < 1$, where N_S is the average number of photons per mode. Its initial CM is equivalent to that in Eq. (1).

Consider the action of a generic Gaussian channel with transmissivity τ, and excess noise ϵ on a single mode A of an arbitrary input TMSV state with CM $\gamma_{A,B}$. The output CM is given by

$$\gamma'_{A,B} = \begin{pmatrix} \tau(V+B+\epsilon)\mathbf{1} & \sqrt{\tau(V^2-1)}\mathbf{Z} \\ \sqrt{\tau(V^2-1)}\mathbf{Z} & V\mathbf{1} \end{pmatrix}, \tag{5}$$

where $V = (1+\lambda^2)/(1-\lambda^2)$ is the variance of the thermal state $\mathrm{Tr}_A\,|\lambda\rangle\langle\lambda|$ and $B = (1-\tau)/\tau$ is the input equivalent noise due to losses.

Now consider the implementation of a NLA to mode A prior to measurement. It can be shown that [21] the CM $\gamma'_{A,B}(\lambda,\tau,\epsilon,g)$ of the amplified state, post NLA action, is equivalent to the CM $\gamma'_{A,B}(\lambda^g,\tau^g,\epsilon^g,g=1)$ of an equivalent system with TMSV parameter λ^g, under action of a Gaussian channel with transmissivity τ^g and excess noise ϵ^g, without the use of an NLA. These effective parameters are given by

$$\begin{aligned} \lambda^g =& \lambda\sqrt{\frac{(g^2-1)(\epsilon-2)\tau-2}{(g^2-1)\epsilon\tau-2}}, \\ \tau^g =& \frac{g^2\tau}{(g^2-1)\tau\left(\frac{1}{4}(g^2-1)(\epsilon-2)\epsilon\tau-\epsilon+1\right)+1}, \\ \epsilon^g =& \epsilon - \frac{1}{2}(g^2-1)(\epsilon-2)\epsilon\tau. \end{aligned} \tag{6}$$

For the above system of effective parameters to represent an actual physical system, the following constraints must be satisfied: $0 \le \lambda^g < 1$, $0 \le \tau^g \le 1$ and $\epsilon^g \ge 0$. The first is always satisfied when

$$0 \le \lambda^g < 1 \Rightarrow 0 < \lambda < \left(\sqrt{\frac{(g^2-1)(\epsilon-2)\tau-2}{(g^2-1)\epsilon\tau-2}}\right)^{-1}. \tag{7}$$

The second and third conditions are satisfied provided the excess noise $\epsilon < 2$ and the gain is smaller than a maximum value given by

$$g_{\max} = \sqrt{\frac{\epsilon(\tau(\epsilon-4)+2)+4\sqrt{\frac{\tau(\epsilon-2)+2}{\epsilon}}-2\sqrt{\epsilon(\tau(\epsilon-2)+2)}+4\tau-4}{\tau(\epsilon-2)^2}}. \tag{8}$$

Equivalences can be made between Eq. (5) and Eq. (3): For QI we consider a TMSV state with N_S mean photons per mode such that the variance $V = 2N_S+1$ and $\sqrt{V^2-1} = 2\sqrt{N_S(N_S+1)}$ while Gaussian channel transmissivity $\tau \equiv \kappa$, the target reflectivity. Of course, for real-world target detection this parameter would also incorporate other losses and gains given by the radar equation. In QI, a portion κ of the signal is mixed with the thermal background, which comprises $N_B/(1-\kappa)$ mean photons per mode. Taking into account this rescaling, when the target is present the returning signal mode takes the form

$$\begin{aligned} &\kappa(2N_S+1)+(1-\kappa)\left(\frac{2N_B}{1-\kappa}+1\right) \\ &\equiv \tau V + B\tau\left(\frac{2N_B}{1-\tau}+1\right) \\ &= \tau\left(V+B+\frac{2N_B}{\tau}\right) \equiv \tau(V+B+\epsilon), \end{aligned} \tag{9}$$

where excess noise has a simple relation with N_B given by $\epsilon = \frac{2N_B}{\tau} \equiv \frac{2N_B}{\kappa}$. Thus by considering an equivalent system of effective parameters in place of the two conditional CMs for QI given in Eqs. (2) and (3), one can consider the additional action of an NLA on the returning signal modes at the receiver, before joint measurement with the retained idler.

Note that the constraint on excess noise to maintain the effective system's physicality means that $\epsilon = \frac{2N_B}{\kappa} < 2$, i.e., $N_B < \kappa$. Since $0 \le \kappa \le 1$, we have the global constraint $N_B < 1$ on the mean number of thermal photons associated with the background. Typically, for QI, the parameter constraints involve very high background, $N_B \gg 1$, which is naturally satisfied in the microwave domain at room temperature, and $\kappa \ll 1$. However these are not strictly necessary for a quantum advantage exists; provided $N_S \ll 1$ quadrature correlations c_q are maximised and it is from here where the quantum advantage arises. The new constraint on N_B introduced here means that, comfortably, at room temperature ($T = 300$K) applications the protocol described here is valid for frequencies $\gtrsim$ 4THz, beginning at the higher end of the microwave. Lower frequencies can meet this requirement as long as the temperature of application is small enough, e.g., for operations at $\sim$ 1GHz we require $T \lesssim 0.07$K.

Further, for a given environment (N_B) and target parameters (κ), Eq. (7) implies that the maximum value of signal energy, N_S, which may be employed is given by

$$N_S^{\max}(g) = \frac{1-N_B(g^2-1)}{\kappa(g^2-1)}, \tag{10}$$

which is maximised when $g = 1$, i.e., no amplification occurs and the protocol is equivalent to that of standard QI.

The action of the NLA is a non-deterministic one. That is, it provides a tool for heralded noiseless quantum amplification, i.e., ideally, the transformation $|\alpha\rangle \to |g\alpha\rangle$, where $g > 1$ is the NLA gain, with some probability of success, $P(g)$ [14–16]. In other words, under NLA action the number of probings used for the detection process transforms as $M \to MP(g)$ with the remaining $M(1-P(g))$ channel uses discarded. Thus, with NLA action we are considering post-selected QI and the problem of hypothesis testing becomes one of two stages and four potential outcomes:

H_{00} : Target is absent, and the NLA is unsuccessful;

H_{01} : Target is absent, and the NLA is successful;

H_{10} : Target is present, and the NLA is unsuccessful;

H_{11} : Target is present, and the NLA is successful.

Post-selection essentially discards all events corresponding to hypotheses H_{00} and H_{10} and the problem is reduced to standard QI involving the discrimination of only two hypotheses H_{01} and H_{11}, subject to $M \to MP(g)$.

C. Classical benchmarking with coherent states

In the absence of an idler the best strategy is to use coherent states. The signal is prepared in the coherent state $|\sqrt{2N_S}\rangle$ which is then sent out to some target region. Under H_0, the received returning mode is in a thermal state with mean photon number N_B and CM equal to $\omega\mathbf{1}$, i.e., $\hat{a}_R = \hat{a}_B$. Under H_1, the signal is mixed with the background such that $\hat{a}_R = \sqrt{\kappa}\hat{a}_S + \sqrt{1-\kappa}\hat{a}_B$ with $\kappa \in (0,1)$, corresponding to a displaced thermal state with mean vector $(\sqrt{2\kappa N_S}, 0)$ and CM $\omega\mathbf{1}$.

Consider the thermal state $\hat{\rho}_{\rm th}(\lambda_{\rm th})$ with Fock basis representation

$$\hat{\rho}_{\rm th}(\lambda_{\rm th}) = (1-\lambda_{\rm th}^2)\sum_{n=0}^{\infty}\lambda_{\rm th}^{2n}\,|n\rangle\langle n|\,, \tag{11}$$

displaced by complex β yielding the state $\hat{\rho} = \hat{D}(\beta)\hat{\rho}_{\rm th}(\lambda_{\rm th})\hat{D}(-\beta)$. Such a state can be written as an ensemble of coherent states,

$$\hat{\rho} = \int P(\alpha)\,|\alpha\rangle\langle\alpha|\,{\rm d}\alpha, \tag{12}$$

where $P(\alpha) = \frac{e^{|\alpha|^2}}{\pi^2}\int e^{|u|^2}\langle -u|\hat{\rho}|u\rangle e^{u^\star\alpha - u\alpha^\star}{\rm d}u$, is the P-function [21].

After successful amplification, realised by the operator $\hat{C} = g^{\hat{n}}$ where $\hat{n}$ is the Fock basis number operator, the coherent state $|\alpha\rangle$ transforms as

$$\hat{C}\,|\alpha\rangle = e^{\frac{|\alpha|^2}{2}(g^2-1)}|g\alpha\rangle \tag{13}$$

such that the initial state after NLA action becomes

$$\hat{\rho}' = \hat{C}\hat{\rho}\hat{C} = \int P(\alpha)e^{|\alpha|^2(g^2-1)}\,|g\alpha\rangle\langle g\alpha|\,{\rm d}\alpha. \tag{14}$$

After change of variables it can be found that the resulting state after NLA action obeys the following relation of proportionality:

$$\hat{\rho}' \propto \hat{D}(\bar{g}\beta)\hat{\rho}_{\rm th}(g\lambda_{\rm th})\hat{D}(-\bar{g}\beta), \tag{15}$$

where $\bar{g} = g(1-\lambda_{\rm th}^2)/(1-g^2\lambda_{\rm th}^2)$. That is, as in the case for a TMSV source, the result of a displaced thermal state acted on by an NLA is equivalent to a displaced thermal state with modified effective parameters without amplification, subject to the constraint that $g\lambda_{\rm th} < 1$ to ensure physicality.

For QI applications, the initial coherent state $\left|\sqrt{2N_S}\right\rangle$ is sent through a quantum channel with reflectivity/transmittance κ such that the displacement can be taken as $\beta = \sqrt{2\kappa N_S}$. Meanwhile, the variance of the thermal state is given by

$$\frac{1+\lambda_{\rm th}^2}{1-\lambda_{\rm th}^2} = 2N_B + 1 = \omega \Rightarrow \lambda_{\rm th}^2 = \frac{N_B}{1+N_B}. \tag{16}$$

Thus, action of the NLA on the displaced thermal state with these parameters yields the following transformations: for the mean,

$$\begin{aligned}\sqrt{2\kappa N_S} &\to g\frac{1-\lambda_{\rm th}^2}{1-g^2\lambda_{\rm th}^2}\sqrt{2\kappa N_S}\\ &= \frac{g}{1+N_B(1-g^2)}\sqrt{2\kappa N_S} = \beta'.\end{aligned} \tag{17}$$

Then,

$$\lambda_{\rm th}^2 = \frac{N_B}{1+N_B} \to g^2\frac{N_B}{1+N_B} = \lambda_{\rm th}'^2, \tag{18}$$

such that the effective variance becomes

$$\frac{1+\lambda_{\rm th}'^2}{1-\lambda_{\rm th}'^2} = \frac{1+N_B(1+g^2)}{1+N_B(1-g^2)} = \omega'. \tag{19}$$

D. Performance bounds for QI with NLA

1. TMSV state with NLA

Using the tools of App. A the QCB of the maximally-entangled TMSV source for QI may be computed. This is done using mathematical computational software, the full form too long to be exhibited here, but its behaviour is plotted in Figs. 2 and 3 and discussed in Sec. II E.

2. Coherent state with NLA

As with the TMSV source, the tools of App. A may be used to compute the QCB of a coherent state with amplification by considering an equivalent protocol, without amplification, using modified effective parameters for mean and variance given by Eqs. (17) and (19), respectively. For equally-likely hypotheses, the single-use ($M = 1$) QCB for a coherent state with NLA amplification takes the exact form

$$P_{\rm CS+NLA}^{{\rm QCB},M=1} \le \frac{1}{2}\exp\left(-\frac{g^2\kappa N_S\left(\sqrt{N_B+1}-g\sqrt{N_B}\right)^2}{(1+N_B-g^2N_B)^3}\right), \tag{20}$$

assuming successful amplification for that single use.

Taking into account the number of successful probings used to achieve this bound, each occurring with probability of success $P(g)$, we have for a total of M-uses, with

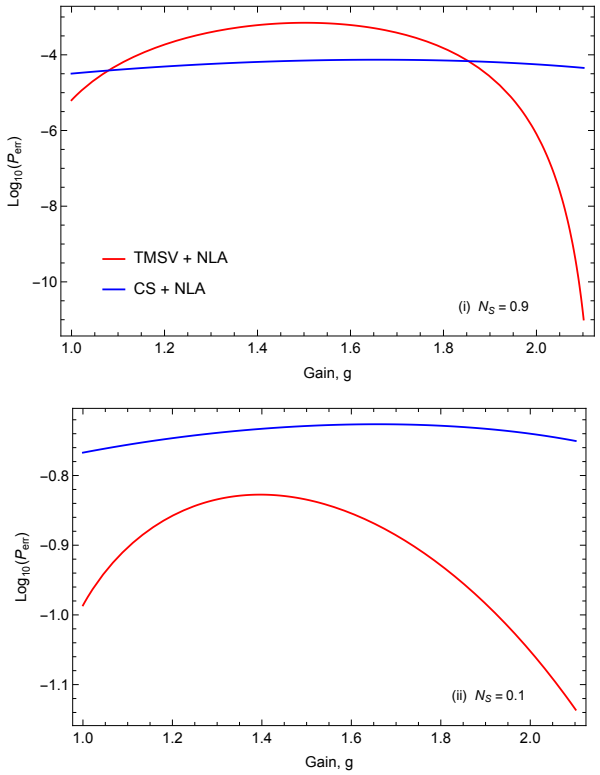

FIG. 2: Error probability exponents for QI using a maximally-entangled TMSV source with NLA (red) at the receiver, compared to a coherent state source with the same NLA (blue) as a function of NLA gain, g. In both panels, parameters are set such that $N_B = 0.1$, $\kappa = 0.2$ such that the maximum source energy applicable across the range, $N_S^{\max}(g_{\max}) \simeq 0.96$. Thus, values are plotted for (i) $N_S = 0.9$ and (ii) $N_S = 0.1$. The total number of probes $M = 100$.

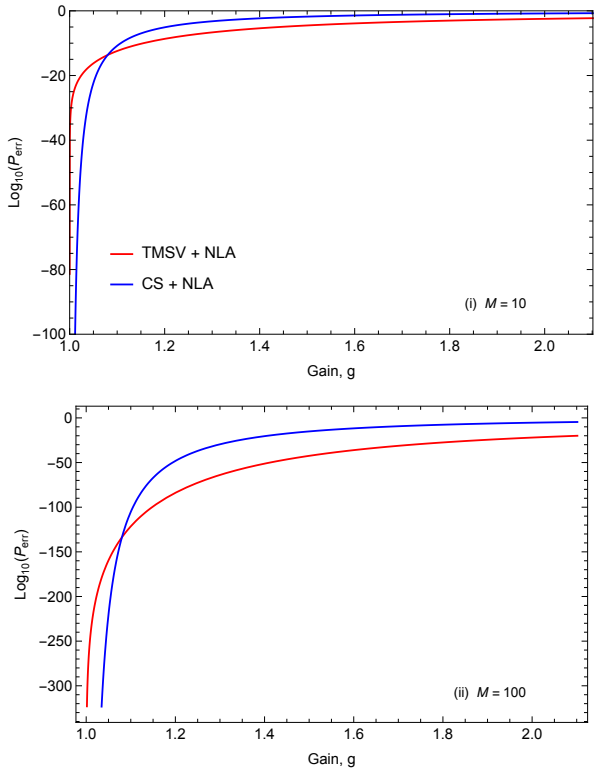

FIG. 3: Error probability exponents for QI using a maximally-entangled TMSV source with NLA (red) at the receiver, compared to a coherent state source with the same NLA (blue) as a function of NLA gain, g. In both panels, parameters are set such that $N_B = 0.1$, $\kappa = 0.2$, while for each value of g, the signal energy is set very close (99%) to its local maximum, i.e., $N_S = N_S^{\max}(g)$. Total number of probes is set to for (i) $M = 10$ and (ii) $M = 100$.

$M > 1$,

$$P_{\mathrm{CS+NLA}}^{\mathrm{QCB}} \leq \frac{1}{2}\exp\left(-\frac{MP(g)g^2\kappa N_S\left(\sqrt{N_B+1}-g\sqrt{N_B}\right)^2}{(1+N_B-g^2N_B)^3}\right), \quad (21)$$

with similar consideration employed in the computation of the TMSV + NLA QCB in Sec. II D 1.

The QCB of such a coherent state transmitter, without amplification, may be readily computed and takes the exact form [9]

$$P_{\mathrm{CS}}^{\mathrm{QCB}} \leq \frac{1}{2}\exp\left(-M\kappa N_S\left(\sqrt{N_B+1}-\sqrt{N_B}\right)^2\right). \quad (22)$$

Regimes for which the use of an NLA yields a performance enhancement in coherent state protocols is studied and discussed in detail in Sec. II F.

E. Benchmarking QI with NLA

1. *Comparison of NLA protocols*

Since the coherent state forms the ideal, minimum-uncertainty state and serves as the theoretically optimal classical benchmark, Eq. (21) allows for the benchmarking of the TMSV with the use of an NLA for target detection.

Taking into account constraints on effective parameters given by Eq. (6), Figs. 2 and 3 plot the performance of the TMSV state with NLA relative to that of a coherent state with NLA. Note that the full, exact forms of the QCB have been employed in the computation, that is, without any assumptions as to the relative magnitude of parameter values. Further, the plots have been generated assuming a maximum theoretical probability of success, given by $P(g) = 1/g^2$ to model the absolute limits of NLA performance.

In Fig. 2, the error probability exponent is plotted as function of the NLA gain, g, up to and including $g_{\max}$, for fixed environmental parameters $N_B = 0.1$ and $\kappa = 0.2$

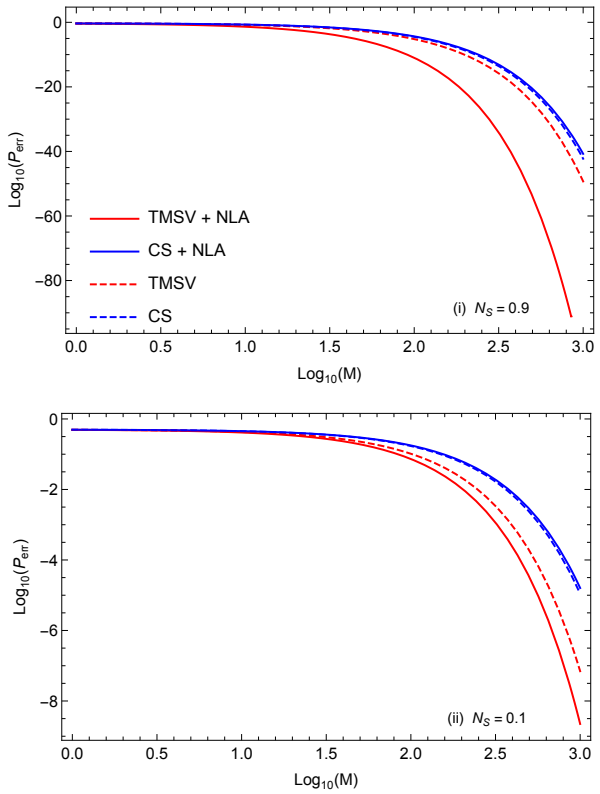

FIG. 4: Error probability exponents for QI using a maximally-entangled TMSV source with NLA (red, solid) at the receiver, compared to a coherent state source with the same NLA (blue, solid) as a function of the number of probes, M. Also included are performance bounds without the use of the NLA (dashed). In both panels, parameters are set such that $N_B = 0.1$, $\kappa = 0.2$ such that the maximum source energy applicable across the range, $N_S^{\max}(g_{\max}) \simeq 0.96$, with $g = g_{\max} \simeq 2.1$. Thus, values are plotted for (i) $N_S = 0.9$ and (ii) $N_S = 0.1$.

with the total number of probings $M = 100$. Based on these parameters it can be found that the maximum energy valid across all values of g, maintaining physicality, is given by $N_S^{\max}(g_{\max}) \simeq 0.96$ thus results are plotted for two values of N_S: 0.9 and 0.1. It can clearly be seen that an increase in the gain, g, has a much larger and more valuable effect on the the TMSV state, compared to the same amplification of the returning coherent state. Note that where $g = 1$ the performance coincides with that of the standard QI protocol without any amplification. As expected, smaller values of source energy N_S are favoured by the QI with a TMSV source compared to the coherent state since it is for small N_S where cross-correlations, $c_q = 2\sqrt{N_S(N_S+1)}$, are maximised.

Fig. 3 plots the same function as Fig. 2 with much of the same parameters, however in this scenario rather than considering the global maximum of N_S, applicable across all values of g, up to and including $g_{\max}$, we consider a source whose energy is given by (99% of) the local maximum. That is, for each value of $g \in [0, g_{\max}]$, N_S is set such that $N_S = N_S^{\max}(g)$. Of course, $N_S^{\max}$

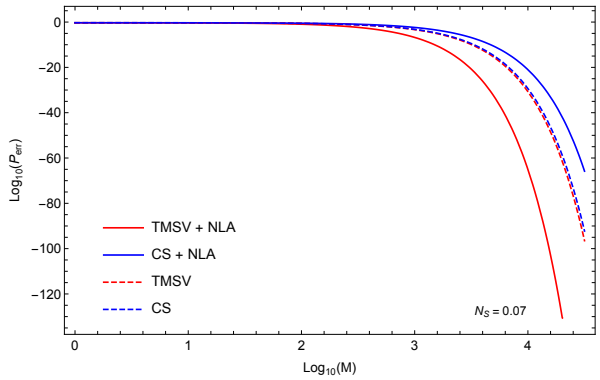

FIG. 5: Error probability exponents for QI using a maximally-entangled TMSV source with NLA (red, solid) at the receiver, compared to a coherent state source with the same NLA (blue, solid) as a function of the number of probes, M. Also included are performance bounds without the use of the NLA (dashed). In both panels, parameters are set such that $N_B = 0.005$, $\kappa = 0.1$ such that the maximum source energy applicable across the range, $N_S^{\max}(g_{\max}) \simeq 0.075$, with $g = g_{\max} \simeq 11$. Values are plotted for $N_S = 0.07$.

is a decreasing function of g so the behaviour observed for $g \to 1$, where N_S is typically very large, the coherent state outperforms the TMSV. However small increases in g show a large quantum advantage can be achieved, even at the maximal N_S value. This quantum advantage may be amplified in cases where the source energy must be kept low, as in stealth surveillance or biomedical sensing where samples may be sensitive to high energies, due to the freedom available in decreasing N_S below the value used in this comparison. Making use of such freedom will, of course, amplify entanglement benefits.

2. *Comparison with non-NLA protocols*

While Sec. II E 1 shows that the use of NLAs yields improvement in performance for TMSV protocols over coherent state protocols, there is, of course, a question as to whether or not their use is beneficial when one can simply forgo the NLA and keep all M channel uses in the detection. After all, successful amplification comes at the expense of a proportion, QCBs for target detection, both for QI with a TMSV source and coherent states (see Ref. [10] for full details), may be recovered by simply setting $g = 1$.

Figs. 4 and 5 plot the error probability exponents for QI using a maximally entangled TMSV source with an NLA at the receiver alongside that of a coherent state source using the same NLA. For comparison and to show that the NLA is of actual value, we plot the QCBs for the same protocols without the use of the NLA. In these protocols all M probings are used at the receiver in decision-making. Results show that there exists a clear advantage in employing NLAs at the receiver compared to without.

Note that Figs. 2 and 3 are given to qualitatively show

	Fig. 4(i)	Fig. 4(ii)	Fig. 5
$P^{\rm QCB}_{\rm QI+NLA} \lesssim$	0.00044^{ϵ_1}	0.0033^{ϵ_1}	0.000092^{ϵ_2}
$P^{\rm QCB}_{\rm CS+NLA} \lesssim$	0.44^{ϵ_1}	0.91^{ϵ_1}	0.30^{ϵ_2}
$P^{\rm QCB}_{\rm QI} \lesssim$	0.37^{ϵ_1}	0.87^{ϵ_1}	0.17^{ϵ_2}
$P^{\rm QCB}_{\rm CS} \lesssim$	0.43^{ϵ_1}	0.91^{ϵ_1}	0.19^{ϵ_2}

TABLE I: QCBs for both QI and coherent state illumination when $M = 10^6$ for the parameter regimes considered in Figs. 4 and 5. The QCB is given in the form x^{ϵ}, where for Fig. 4, $\epsilon = \epsilon_1 \simeq 113214$, and for Fig. 5, $\epsilon = \epsilon_2 \simeq 4000$.

the behaviour of NLA performance for each of the two considered Gaussian sources, as a function of NLA gain, when considering variations in system parameters. Of course, the use of the QCB for evaluation of error probabilities in problems like target detection is only truly valid in the limit of a large number of uses, i.e., $M \gg 1$.

Numerical limitations render the inclusion of such large values in the plots not possible however, by considering error probabilities at $M = 10^6$, it can be seen that the observed behaviours persist. The associated QCBs in this limit are given in Table I.

F. Quantum-inspired coherent state target detection with an NLA

Comparing the error-exponents of Eqs. (22) and (21) allows for the conditions under which an advantage in using an NLA for coherent state illumination to be determined in the limit of $M \gg 1$.

Broadly speaking, for arbitrary $P(g)$, there are two physical regimes where this occurs: the first coincides with the operation in the optical domain where an advantage is possible for all $P(g) > 0$ when $N_B = 0$ and gain, $g \geq \sqrt{1/P(g)}$. Note that this recovers the theoretical upper bound on the probability of success for the NLA [14–16], that is, $P(g) \leq 1/g^2$. The second regime, valid for non-zero background, $N_B > 0$, as studied here, provides a global upper bound on possible values of NLA gain yielding an advantage given by $g < \sqrt{(1+N_B)/N_B}$. Further, there exists a lower bound given by the root of a polynomial dependent also on N_B and $P(g)$.

For simplicity, let us assume that our NLA operates with maximal probability of success such that $P(g) = 1/g^2$. Then, in the limit of large M, the conditions for an NLA advantage using coherent states reduces to

$$\begin{cases} N_B = 0, & \forall g \in \mathbb{R}; \\ 0 < N_B < \frac{1}{3}, & \text{Root}_2\left[\xi\right] \leq g < \sqrt{\frac{1+N_B}{N_B}}; \\ N_B = \frac{1}{3}, & 1 \leq g < 2; \\ N_B > \frac{1}{3}, & 1 \leq g < \sqrt{\frac{1+N_B}{N_B}}, \end{cases} \tag{23}$$

where $\text{Root}_2[\xi]$ denotes the second root of the polynomial

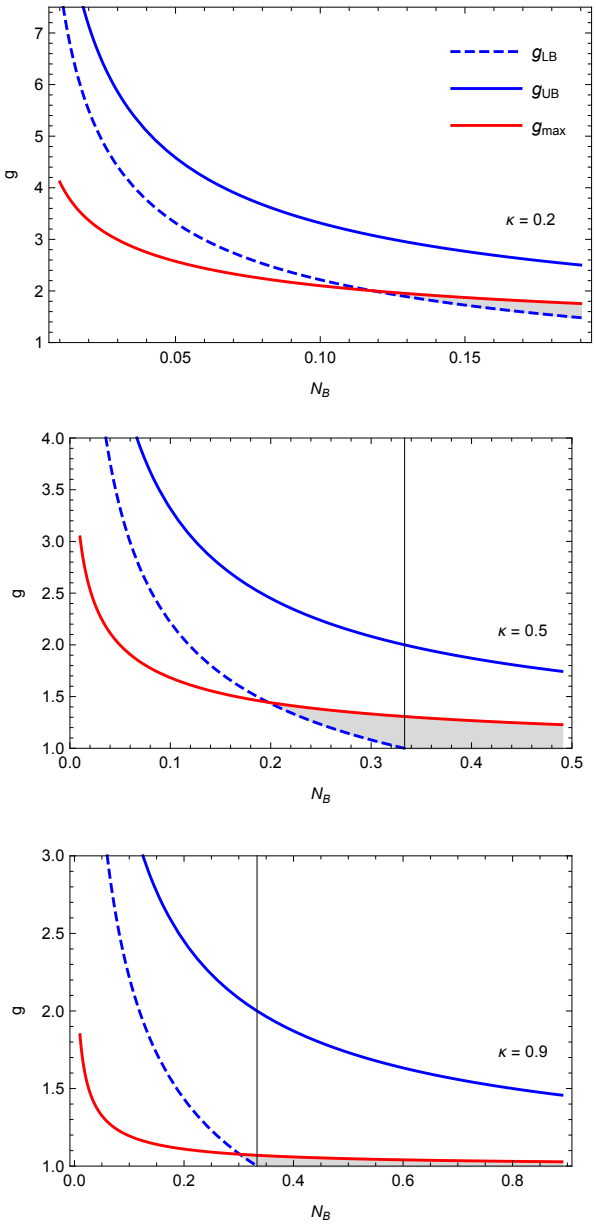

FIG. 6: Conditions for which an advantage may be found in coherent state target detection using an NLA with gain g compared to without, as a function of mean number of background photons per mode, N_B. Each panel shows results for differing values of target reflectivity: $\kappa = 0.2$, $\kappa = 0.5$ and $\kappa = 0.9$. Upper- and lower- bounds of Eq. (23), given by $\sqrt{(1+N_B)/N_B}$ (blue, solid) and $\text{Root}_2[\xi]$ (blue, dashed), respectively, are shown including only values of physical interest where $g \geq 1$. Shaded is the region of valid NLA gain g for which an advantage may be found which is ultimately bounded by $g_{\max} = g_{\max}(N_B, \kappa)$ (red). The border point of Eq. (23) where $N_B = 1/3$ is also shown (black, vertical).

equation $\xi = 0$, with

$$\begin{aligned}\xi = \xi(g, N_B) &= -4 - 4N_B + N_B^3 \\ &+ (8N_B + 8N_B^2 + 2N_B^3)g + (8N_B + 4N_B^2 - N_B^3)g^2 \\ &+ (-8N_B^2 - 4N_B^3)g^3 + (-4N_B^2 - N_B^3)g^4 \\ &+ 2N_B^3 g^5 + N_B^3 g^6.\end{aligned} \tag{24}$$

Given in Eq. (23) are only conditions whose parameter values are physically possible. Note, also, the conditions imposed by the methodology used here, demanding that $N_B < \kappa \Rightarrow N_B < 1$. As a result, the last condition, valid for any $1/3 < N_B < 1$ becomes $\sqrt{2} < g \leq 2$. Meanwhile, for small background values, $0 < N_B < 1/3$, g initially appears to potentially be arbitrarily large. On the other hand, and, again, as a result of the methodology used here, Eq. (8) stipulates that for a given regime, characterised in terms of N_B and κ, there exists a maximum gain, $g_{\max}$, which physically cannot coincide with the upper bounds given in Eq. (23). Further, since $g_{\max}$ is a decreasing function of κ any potential regime for an advantage with the NLA quickly diminishes when κ is increased. Fig. 6 shows qualitatively these behaviours for increasing values of κ and shades regions of NLA gain, subject to constraints and bounds of Eq. (23) for which an advantage may be found. Thus, while the NLA can provide an advantage for coherent states, the regions in which this is possible constrained to limited values of NLA gain g, a constraint which does not exist for the TMSV state. This has been shown in previous sections and results for parameter regimes wherein the use of an NLA for a coherent state protocol is not advantageous. Nonetheless, the NLA gain is a parameter which may be completely controlled experimentally and, as such, could provide a means of enhancement in a quantum-inspired target detection protocol using a semi-classical coherent state source alongside a quantum mechanical receiver comprising an NLA.

In a similar manner to Sec. II E, it is possible to now study regimes in which a quantum-inspired coherent state protocol using an NLA yields an enhancement in target detection. This will be done considering the three non-optical, i.e., for $N_B > 0$, regimes outlined in the conditions of Eq. 23.

Fig. 7 plots the error probability exponents, found via the QCB, for quantum target detection in regimes where the use of an NLA at the receiver yields an advantage for the coherent state source. The results show that while the regimes in which such an advantage is possible are limited, the potential gain in the limit of a large number of uses is significant, by many orders of magnitude. Further, as can be seen in Fig. 7(b), the NLA allows the coherent state to even surpass the TMSV state in performance. Though all cases show that a TMSV state source with the same NLA remains advantageous and outperforms the corresponding semi-classical protocol.

Note that, as before, numerical limitations mean that large values of M, where the QCB is considered valid, cannot be included in the plots of Fig. 7. But, consideration of the error probabilities at $M = 10^6$ show that the behaviours and gaps in performance observed persist for $M \gg 1$.

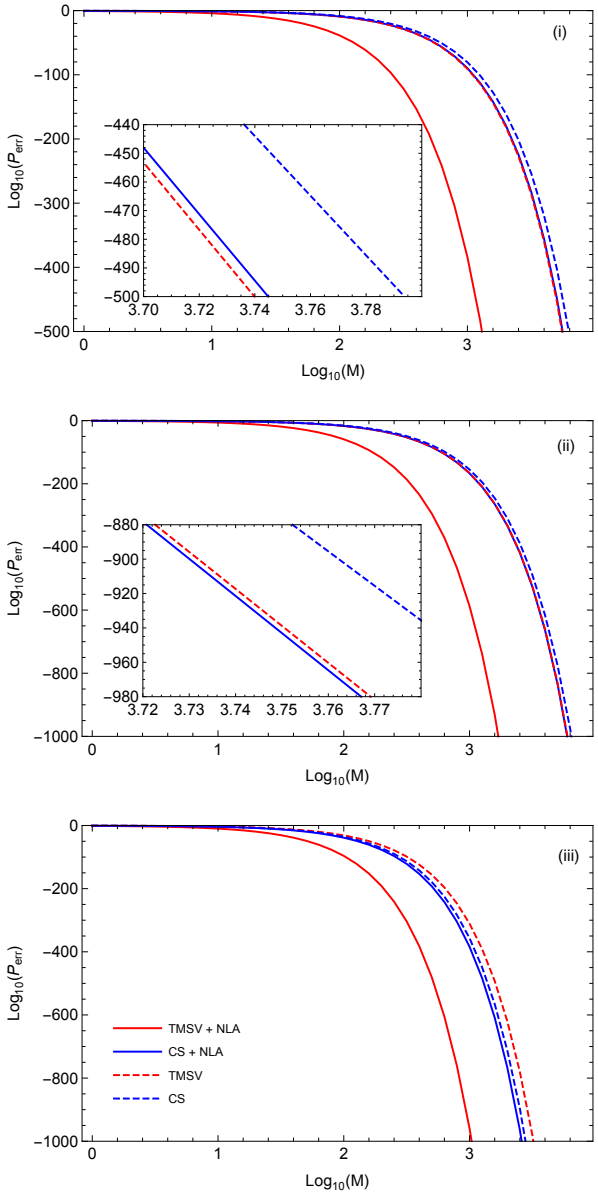

FIG. 7: Error probability exponents for quantum target detection in regions where there is an advantage for coherent states with an NLA (blue, solid) compared to its corresponding non-NLA (blue, dashed) protocol. Also included are performance bounds for the TMSV state both with an NLA (red, solid) and without (red, dashed). For all panels, signal energy is set very close (99%) to the regime's maximum, i.e., $N_S = N_S^{\max}(g_{\max})$, setting $g = g_{\max}$, for parameters: (a) $N_B = 0.25$, $\kappa = 0.3$; (b) $N_B = 1/3$, $\kappa = 0.5$; and (c) $N_B = 0.6$, $\kappa = 0.7$.

III. CONCLUSION

This paper has implemented the action of an NLA at the detection stage of the QI protocol for the purposes od quantum target detection. By mapping the resultant protocol to an equivalent one without the use of an NLA but modified effective parameters, the QCB for symmetric quantum hypothesis testing has been computed. This has been done for both the maximally-entangled TMSV state and the theoretically optimal classical benchmark, the coherent state, with comparisons made between the two assuming a theoretically maximal probability of success for the NLA.

Results show that the employment of non-Gaussian receivers for Gaussian sources in quantum target detection can be beneficial. In particular, an improvement in effective signal-to-noise ratio, resulting in a diminished error probability in target detection, occurs when the NLA is used with a TMSV source. This improvement, however, does not occur when the Gaussian source is the semi-classical coherent state; in this case, the performance is almost always bounded by the coherent state performance when no NLA is used which, in for applications in the optical domain, may be achieved through homodyne detection. Despite this, particular regimes and conditions for NLA gain are provided for which an enhancement in target detection may be achieved with such a semi-classical source; these results suggest a potential quantum-inspired target detection protocol based on experimentally accessible coherent state sources with an NLA. Such a protocol allows for improvements in target detection that are, in some regimes, surpassing the performance of the TMSV state without an NLA.

The mapping used to compute the bounds results in a system of effective parameters for which a quantum advantage is not typically possible in a non-NLA protocol. At least, within such a regime the maximal advantage in error exponent certainly falls short of the potential value of 6 dB. Remarkably, the use of an NLA, even when limited to such a regime, still amplifies the performance of the TMSV state thereby extending the scope of of applicability of QI-based quantum target detection.

Acknowledgments. This work has been funded by the European Union's Horizon 2020 Research and Innovation Action under grant agreement No. 862644 (FET-Open project: Quantum readout techniques and technologies, QUARTET). AK acknowledges sponsorship by EPSRC Award No. 1949572 and Leonardo UK. M.G. would like to acknowledge funding from the European Unions Horizon 2020 research and innovation program under grant agreement No 820466 (Continuous Variable Quantum Communications, 'CiViQ').

[1] D. P. DiVincenzo, *Quantum computation*, Science 270(**5234**), 255-261 (1995).
[2] R. Raussendorf and H. J. Briegel, *A one-way quantum computer*, Phys. Rev. Lett. 86(**22**), 5188 (2001).
[3] H. J. Briegel, D. E. Browne, W. Dür, R. Raussendorf and M. Van den Nest, *Measurement-based quantum computation*, Nat. Phys. 5(**1**), 19-26 (2009).
[4] N. Gisin and R. Thew, *Quantum communication*, Nat. Phot. 1(**3**), 165-171 (2007).
[5] M. Hillery, V. Bužek and A. Berthiaume, *Quantum secret sharing*, Phys. Rev. A 59(**3**), 1829 (1999).
[6] S. Pirandola *et al.*, *Advances in Quantum Cryptography*, Adv. Opt. Photon. 12(**4**) 1012-1236, (2020).
[7] S. Pirandola, B. R. Bardhan, T. Gehring, C. Weedbrook and S. Lloyd, *Advances in photonic quantum sensing*, Nat. Photon. **12**, 724–733 (2018).
[8] S. Lloyd, *Enhanced sensitivity of photodetection via quantum illumination*, Science 321**5895**, 1463-1465 (2008).
[9] S.-H. Tan *et al.*, *Quantum illumination with Gaussian states*, Phys. Rev. Lett. **101**, 253601 (2008).
[10] A. Karsa, G. Spedalieri, Q. Zhuang and S. Pirandola, *Quantum illumination with a generic Gaussian source*, Phys. Rev. Res. **2**, 023414 (2020).
[11] S. Guha and B. I. Erkmen, *Gaussian-state quantum-illumination receivers for target detection*, Phys. Rev. A 80(**5**), 052310 (2009).
[12] Q. Zhuang, Z. Zhang, and J. H. Shapiro, *Optimum mixed-state discrimination for noisy entanglement-enhanced sensing*, Phys. Rev. Lett. 118(**4**), 040801 (2017).
[13] C. M. Caves, *Quantum limits on noise in linear amplifiers*, Phys. Rev. D **26**, 1817 (1982).
[14] C. M. Caves, J. Combes, Z. Jiang, and S. Pandey, *Quantum limits on phase-preserving linear amplifiers*, Phys. Rev. A **86**, 063802 (2012).
[15] T. C. Ralph and A. P. Lund, *Nondeterministic noiselesslinear amplification of quantum systems*, AIP Conference Proceedings **1110**, 155-160 (2009).
[16] S. Pandey, Z. Jiang, J. Combes, and C. M. Caves, *Quantum limits on probabilistic amplifiers*, Phys. Rev. A **88**, 033852 (2013).
[17] M. Barbieri, F. Ferreyrol, R. Blandino, R. Tualle-Brouri, and P. Grangier, *Nondeterministic noiseless amplification of optical signals: a review of recent experiments*, Laser Phys. Lett. **8**, 411 (2011).
[18] F. Ferreyrol, M. Barbieri, R. Blandino, S. Fossier, R. Tualle-Brouri, and P. Grangier, *Implementation of anondeterministic optical noiseless amplifier*, Phys. Rev.Lett. **104**, 123603 (2010).
[19] H. M. Chrzanowski, N. Walk, S. M. Assad, J. Janousek, S. Hosseini, T. C. Ralph, T. Symul, and P. K. Lam, *Measurement-based noiseless linear amplification for quantum communication*, Nat. Photon. **8**, 333-338 (2014).
[20] R. J. Donaldson, R. J. Collins, E. Eleftheriadou, S. M.Barnett, J. Jeffers, and G. S. Buller, *Experimental implementation of a quantum optical state comparison amplifier*, Phys. Rev. Lett. **114**, 120505 (2015).
[21] R. Blandino, A. Leverrier, M. Barbieri, J. Etesse, P. Grangier, and R. Tualle-Brouri, *Improving the maximum transmission distance of continuous-variable quantum key distribution using a noiseless amplifier*, Phys. Rev. A **86**, 012327 (2012).

[22] M. Ghalaii, C. Ottaviani, R. Kumar, S. Pirandola and M. Razavi, *Long-Distance Continuous-Variable Quantum Key Distribution With Quantum Scissors*, IEEE Journal of Selected Topics in Quantum Electronics **26**, 1-12, (2020).

[23] M. Ghalaii, C. Ottaviani, R. Kumar, S. Pirandola and M. Razavi, *Discrete-Modulation Continuous-Variable Quantum Key Distribution Enhanced by Quantum Scissors*, IEEE Journal on Selected Areas in Communications **38**, 506-516 (2020).

[24] B. Xu, C. Tang, H. Chen, W. Zhang, and F. Zhu, *Improving the maximum transmission distance of four-state continuous-variable quantum key distribution by using a noiseless linear amplifier*, Phys. Rev. A **87, 062311** (2013).

[25] J. Dias and T. C. Ralph, *Quantum repeaters using continuous-variable teleportation*, Phys. Rev. A **95**, 022312 (2017).

[26] K. P. Seshadreesan, H. Krovi, and S. Guha, *Continuous-variable quantum repeater based on quantum scissors and mode multiplexing*, Phys. Rev. Research **2**, 013310 (2020).

[27] M. Ghalaii and S. Pirandola, *Capacity-approaching quantum repeaters for quantum communications*, Phys. Rev. A **102**, 062412 (2020).

[28] G. Y. Xiang, T. C. Ralph, A. P. Lund, N. Walk, and G. J. Pryde, *Heralded noiseless linear amplification anddistillation of entanglement*, Nat. Photon. **4**, 316-319 (2010).

[29] Kaushik P. Seshadreesan, Hari Krovi, and Saikat Guha, *Continuous-variable entanglement distillation over a pure loss channel with multiple quantum scissors*, Phys. Rev. A **100**, 022315 (2019).

[30] . J. Zhao, J. Dias, J. Y. Haw, T. Symul, M. Bradshaw, R. Blandino, T. Ralph, S. M. Assad, and P. K. Lam, *Quantum enhancement of signal-to-noise ratio with a heralded linear amplifier*, Optica **4**, 1421-1428 (2017).

[31] C. Weedbrook *et al.*, *Gaussian Quantum Information*, Rev. Mod. Phys. **84**, 621 (2012).

[32] S. Pirandola, *Entanglement Reactivation in Separable Environments*, New J. Phys. **15**, 113046 (2013).

[33] K. Modi, A. Brodutch, H. Cable, T. Paterek and V. Vedral, *The classical-quantum boundary for correlations: Discord and related measures*, Rev. Mod. Phys. **84**, 1655-1707 (2012).

[34] A. Chefles, *Quantum state discrimination*, Contemp. Phys. **41**, 401-424 (2000).

[35] S. M. Barnett and S. Croke, *Quantum state discrimination*, Adv. Opt. Photon. **1**, 238-278 (2009).

[36] A. Chefles, and S. M. Barnett, *Strategies for discriminating between non-orthogonal quantum states*, J. Mod. Opt. **45**, 1295-1302 (1998).

[37] K. M. R. Audenaert *et al.*, *Discriminating States: The Quantum Chernoff Bound*, Phys. Rev. Lett. **98**, 160501 (2007).

[38] J. Watrous, *The theory of quantum information* (Cambridge University Press, Cambridge, 2018).

[39] S. Pirandola and S. Lloyd, *Computable bounds for the discrimination of Gaussian states*, Phys. Rev. A **78**, 012331 (2008).

[40] A. Serafini, F. Illuminati, and S. De Siena, *Symplectic invariants, entropic measures and correlations of Gaussian states*, J. of Phys. B **37**, L21 (2003).

[41] S. Pirandola, A. Serafini, and S. Lloyd, *Correlation matrices of two-mode bosonic systems*, Phys. Rev. A **79**, 052327 (2009).

[42] A. Karsa and S. Pirandola, *Noisy receivers for quantum illumination* IEEE Trans. Aerosp. Electron. Syst. Magazine 5**11**, 22–29 (2020).

[43] S. Pirandola, G. Spedalieri, S. L. Braunstein, N. J. Cerf, and S. Lloyd, *Optimality of Gaussian discord*, Phys. Rev. Lett. 113**14**, 140405 (2014).

Appendix A: The quantum Chernoff bound (QCB)

The binary decision between target absence and presence is reduced to the discrimination of the two quantum states $\hat{\rho}^i_{R,I}$ with $i = 0, 1$ [34–36].

For Gaussian states, closed formulae exist for the computation of bounds on the minimum error probability in quantum state discrimination, such as the quantum Chernoff bound (QCB) [37]

$$P_{\min} \leq P_{\rm QCB} := \frac{1}{2}\left(\inf_{0\leq s\leq 1} C_s\right),$$
$$C_s := \mathrm{Tr}\left[(\hat{\rho}^0_{R,I})^s(\hat{\rho}^1_{R,I})^{1-s}\right], \tag{A1}$$

where the minimisation of the s-overlap C_s occurs over all $0 \leq s \leq 1$. For the problem under study, the minimum is achieved for $s = 1/2$ that corresponds to the simpler quantum Bhattacharyya bound [31]

$$P_{\rm QBB} := \frac{1}{2}\,\mathrm{Tr}\left[\sqrt{\hat{\rho}^0_{R,I}}\sqrt{\hat{\rho}^1_{R,I}}\right]. \tag{A2}$$

Consider two arbitrary N-mode Gaussian states, $\hat{\rho}_0(\mathbf{x}_0, \mathbf{V}_0)$ and $\hat{\rho}_1(\mathbf{x}_1, \mathbf{V}_1)$, with mean $\mathbf{x}_i$ and CM $\mathbf{V}_i$ with quadratures $\hat{\mathbf{x}} = (\hat{q}_1, \hat{p}_1, \ldots, \hat{q}_N, \hat{p}_N)^T$ and associated symplectic form

$$\mathbf{\Omega} = \bigoplus_{k=1}^{N} \begin{pmatrix} 0 & 1 \\ -1 & 0 \end{pmatrix}. \tag{A3}$$

We can write the s-overlap as [39]

$$C_s = 2^N \sqrt{\frac{\det \mathbf{\Pi}_s}{\det \mathbf{\Sigma}_s}} \exp\left(-\frac{\mathbf{d}^T \mathbf{\Sigma}_s^{-1} \mathbf{d}}{2}\right), \tag{A4}$$

where $\mathbf{d} = \mathbf{x}_0 - \mathbf{x}_1$. Here $\mathbf{\Pi}_s$ and $\mathbf{\Sigma}_s$ are defined as

$$\mathbf{\Pi}_s := G_s(\mathbf{V}_0^{\oplus}) G_{1-s}(\mathbf{V}_1^{\oplus}), \tag{A5}$$

$$\mathbf{\Sigma}_s := \mathbf{S}_0 \left[\Lambda_s\left(\mathbf{V}_0^{\oplus}\right)\right] \mathbf{S}_0^T + \mathbf{S}_1 \left[\Lambda_{1-s}\left(\mathbf{V}_1^{\oplus}\right)\right] \mathbf{S}_1^T, \tag{A6}$$

introducing the two real functions

$$G_s(x) = \frac{2^s}{(x+1)^s - (x-1)^s}$$
$$\Lambda_s(x) = \frac{(x+1)^s + (x-1)^s}{(x+1)^s - (x-1)^s}, \tag{A7}$$

calculated over the Williamson forms $\mathbf{V}_i^{\oplus} := \bigoplus_{k=1}^{N} \nu_i^k \mathbf{1}_2$, where $\mathbf{V}_i^{\oplus} = \mathbf{S}_i \mathbf{V}_i^{\oplus} \mathbf{S}_i^T$ for symplectic $\mathbf{S}_i$ and $\nu_i^k \geq 1$ are the symplectic spectra [40, 41].